

Preface

The following is an excerpt from my thesis [Ass15, Chap. 6], slightly edited to allow it to stand on its own as a separate document. It is provided as a supplement to the `WOPTIC` user's guide for the user who wants the gory details of $V_{uv}^\alpha(k)$ interpolation and how it compares to $\mathcal{U}(k)$ interpolation. It should not be considered required reading if you just want to use the package.

Elias Assmann,
September 2015

Woptic: optical conductivity with MLWF

The purpose of the **WOPTIC** package [Ass+15; Wis12] is to calculate the optical conductivity $\sigma_{\alpha\beta}(\Omega)$; its static limit, the dc conductivity $\sigma_{\alpha\beta}(\Omega \rightarrow 0)$; and the Seebeck coefficient or thermopower $S_{\alpha\beta}$ of a periodic interacting electron system. It is integrated rather tightly with **WIEN2k** (to provide the single-particle states and matrix elements between them) and **Wannier90** (to provide a localized basis); interaction effects beyond density-functional theory (DFT) are included via a local self-energy $\Sigma(\omega)$. The self-energy is assumed to be local under the assumption that it comes from a dynamical mean-field theory (DMFT) calculation, but **WOPTIC** is not tied to any specific DMFT implementation.

The distinguishing features of **WOPTIC** are an adaptive tetrahedral grid for the Brillouin zone (**BZ**) integration, and the use of the full momentum matrix elements

$$V_{ab}^{\alpha}(\mathbf{k}) = \langle \psi a\mathbf{k} | \hat{p}_{\alpha} | \psi b\mathbf{k} \rangle \quad (1)$$

in place of a Peierls approximation $V(\mathbf{k}) \approx i \nabla_{\mathbf{k}} H(\mathbf{k})$ [Wis+12]. To avoid clutter, we use natural units throughout, setting the electron's mass and charge as well as the reduced Planck constant to unity: $m_e = e = \hbar = 1$.

The design of the package is such that the management of the adaptive k-mesh is well isolated from the integration routine and other parts of the code. The k-mesh management code was not substantially changed in the course of this dissertation, while the integration routine and various glue and support codes were extended and to a large part rewritten with respect to the original **WOPTIC** package presented in [Wis12]. Therefore, we will focus on these parts and refer to [Ass+15; Wis12] for a description of the adaptive k-mesh refinement. A practical description of **WOPTIC** is provided in the user's guide.

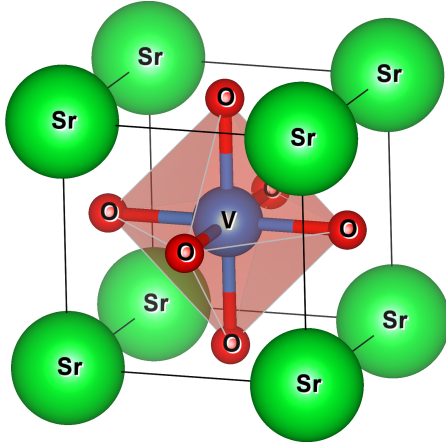


Figure 1: Cubic perovskite crystal structure of SrVO_3 . The O ligands form an octahedron (shown in red) around the V site, leading to the t_{2g} - e_g splitting observed in Fig. 2.

1 Strontium vanadate, testbed material

In the following sections, strontium vanadate (SrVO_3) will be used for all numerical tests. This paramagnetic correlated metal has a cubic perovskite structure, shown in Fig. 1. It is a well studied material, and is often used to showcase new developments in the theory of strongly correlated materials.*

Fig. 2 shows the band structure and density of states of SrVO_3 as computed with WIEN2k using the Perdew-Burke-Ernzerhof (PBE) functional [PBE96]. The three V- t_{2g} -derived bands constitute the low-energy degrees of freedom. They are separated by finite gaps everywhere in the BZ from the O-p states below and the V- e_g states above.

For the purposes of testing WOPTIC, we will use two different types of Wannier projections for SrVO_3 :

- P-3 A 3-band projection on the t_{2g} bands is straightforward. Because the t_{2g} states hybridize with O-p states, the three V-centered orbitals of the resulting “minimal model” for SrVO_3 also have a lot of weight at the O sites [Rib+14].
- P-14 A 14-band projection on the V-d and O-p bands is more delicate because at the R-point, the V- e_g bands become entangled with 3 Sr bands (as seen in Fig. 2). In practice, as long as the R-point is not included in the Wannierization k-mesh, this entanglement can be ignored. (For an isotropic

* To give a few examples, DMFT calculations are presented in [Lie03; Nek+05; Pav+04; Sek+04; Tar+13; Tom+12]; Wannier projections in [Kun+10; Pav+05; Rib+14; Sca+14].

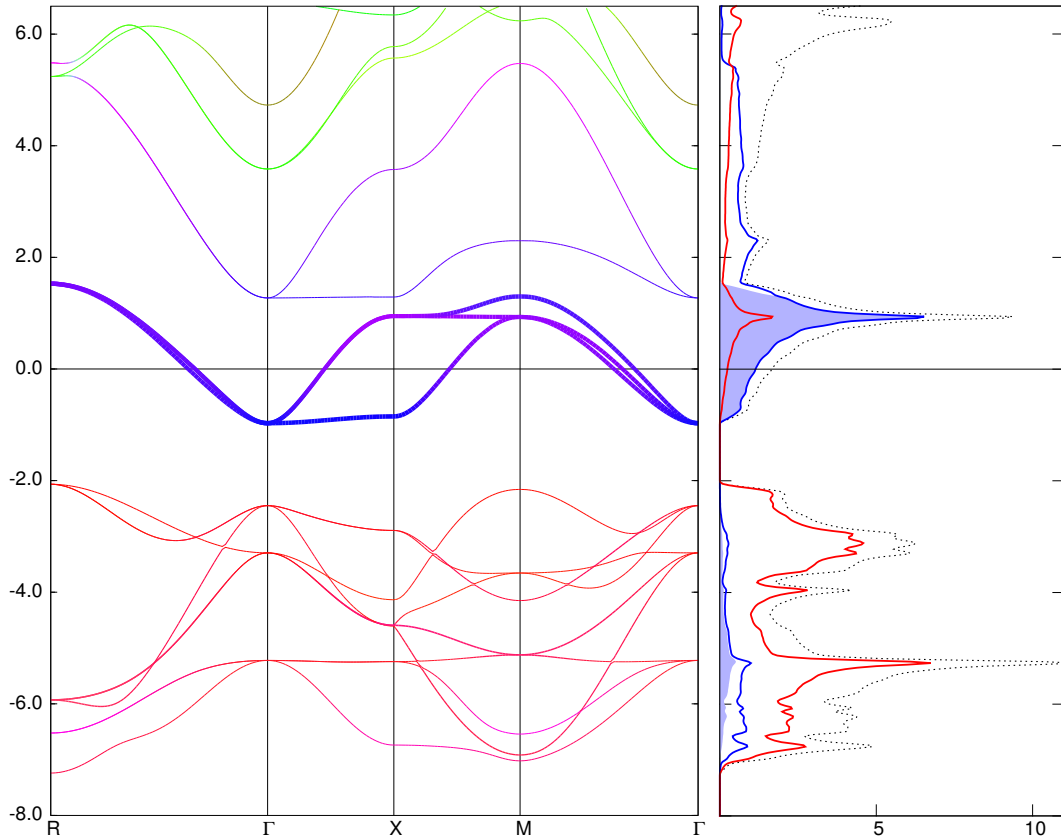


Figure 2: Bandstructure (left) and DOS (right; in states per eV per unit cell) of SrVO_3 . Energy (left scale) is in eV. The contributions are color-coded: red for O, blue for V, green for Sr. On the left, the V-t_{2g} bands are highlighted by thicker lines (i.e., the line width is proportional to the V-t_{2g} weight); on the right, the V-t_{2g} contribution is shaded, and the dotted line represents the total DOS.

$L \times L \times L$ mesh this is the case if L is odd.) Otherwise, disentanglement is expedient to obtain good Wannier functions (wf). In any case, the resulting orbitals are close to the atomic case, since all relevant states are explicitly included in the Wannier projection (i.e. there is little hybridization with any other bands) [Rib+14; Sca+14].

To judge the quality of the different projections, we can compare the respective Wannier-interpolated band structures (Fig. 3). As described above, the $8 \times 8 \times 8$ projection without disentanglement (using the 14 lowest-energy

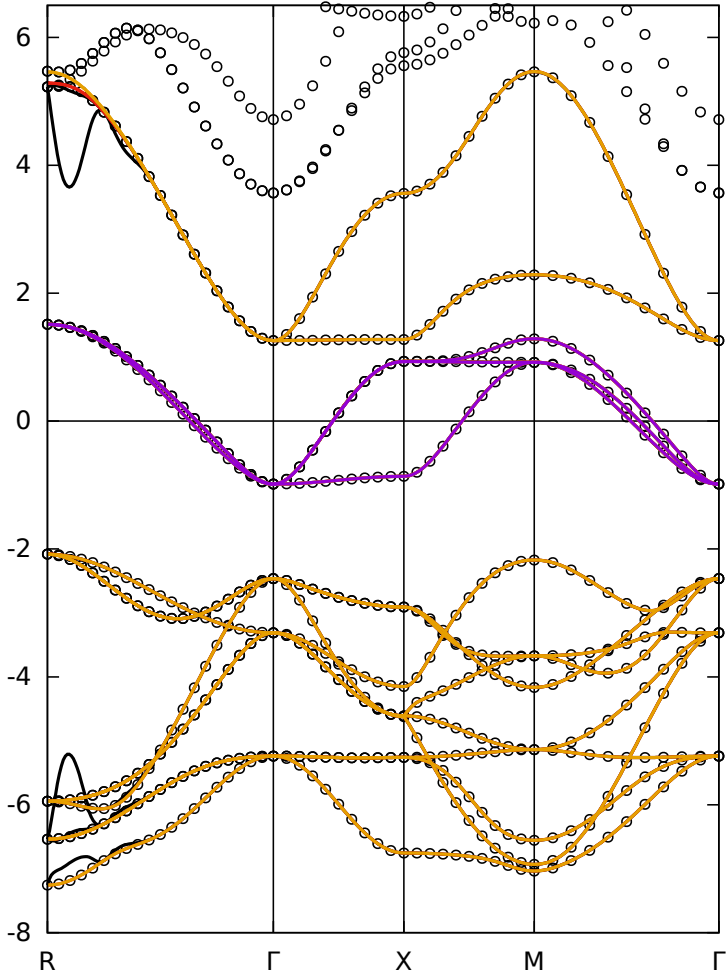


Figure 3: Wannier-interpolated band structures for SrVO_3 from different projections:

- (purple) P-3,
- (red) P-14 without disentanglement on $9 \times 9 \times 9$ k-points,
- (black) the same on $8 \times 8 \times 8$ k-points,
- (orange) P-14 with disentanglement;
- compared to
- (circles) the WIEN2k result.

Throughout most of the BZ, all projections follow the DFT bands closely, such that only one of the lines is visible. The discrepancies between the P-14 projections around R (i.e. the corner point of the BZ) are due to entangled Sr bands (see text).

bands starting from 8 eV below the Fermi level) fails to reproduce the WIEN2k bands around the R -point. Using a $9 \times 9 \times 9$ k-mesh instead, the bands are reproduced faithfully. If an additional 3 bands are included for disentanglement, the Wannier-interpolated bands follow the V character more closely, as a comparison to Fig. 2 reveals. To do so, it must necessarily depart from the WIEN2k bands. This is an illustration of the general rule that the maximally localized Wannier function (MLWF) transformation is no longer unitary when disentanglement is used.

2 Computing the integrand

The optical conductivity $\sigma^{\alpha\beta}(\Omega)$ (in the general case a tensor with $\alpha, \beta \in \{x, y, z\}$) at external frequency Ω may be written as an integral over $k \in \text{BZ}$ and an internal frequency ω [Wis12],

$$\sigma^{\alpha\beta}(\Omega) = \frac{1}{\tau^2} \int_{-\infty}^{+\infty} d\omega w(\omega; \Omega) \int_{\text{BZ}} dk \mathcal{T}^{\alpha\beta}(k, \omega; \Omega) \quad (2)$$

where $\tau = 2\pi$ denotes the circle constant, i.e. the circumference of the unit circle [Har10; Pal01];

$$w(\omega; \Omega) := \frac{f(\omega) - f(\omega + \Omega)}{\Omega} \quad (3)$$

is a weight factor; and the trace

$$\mathcal{T}^{\alpha\beta}(k, \omega; \Omega) := \text{tr}\{A(k, \omega) V^\alpha(k) A(k, \omega + \Omega) V^\beta(k)\} \quad (4)$$

becomes the central quantity in WOPTIC. The purpose of this section is to explain how \mathcal{T} is computed in practice.

In (3), $f(\omega) = (1 + \exp \beta\omega)^{-1}$ is the Fermi-Dirac distribution at inverse temperature β (setting the Fermi level to 0),

$$A(k, \omega) = \frac{i}{\tau}(G(k, \omega) - G^+(k, \omega)) \quad (5)$$

is the spectral function matrix, $V^\alpha(k)$ is the momentum matrix (1), and the trace runs over orbitals and spin. To simplify the notation, we will usually suppress the k -dependence, and adopt the following index conventions: a, b, \dots run over all Bloch states; u, v, \dots over the Wannier states; n, m, \dots over Bloch states inside and i, j, \dots over Bloch states outside of the Wannier window; α, β enumerate the Cartesian directions; and repeated indices imply summation.

The dc conductivity and thermopower can be computed from very similar expressions in the static limit, where

$$w(\omega; \Omega \rightarrow 0) = \frac{\beta/4}{(\cosh \beta\omega/2)^2}. \quad (6)$$

To excite an electronic transition, the photon frequency Ω must connect an empty state to a filled one, i.e. one of ω and $\omega + \Omega$ must be negative and the

other positive, which is enforced by the weight factor (3), modulo temperature broadening. This observation can be exploited to limit the range of ω -integration. Since the external frequency $\Omega \geq 0$, the internal frequency should satisfy

$$-(\Omega + \Delta\omega) < \omega < 0 + \Delta\omega, \quad (7)$$

with $\Delta\omega$ chosen according to temperature and desired accuracy. To include all ω where $w > \varepsilon$, it suffices to set $\Delta\omega$ according to the static limit (6),

$$\cosh \beta \Delta\omega > \sqrt{\frac{\beta}{4\varepsilon}}. \quad (8)$$

This requirement is more stringent than $w < \varepsilon$ would be for any finite Ω , though for realistic values of the variables, the results are very similar.

For practical purposes, we will split (4) into parts inside the Bloch ($\psi\psi$) and Wannier (ww) subspaces, and a mixed term (w ψ):

$$\mathcal{T} = \mathcal{T}_{\psi\psi} + \mathcal{T}_{ww} + \mathcal{T}_{w\psi}. \quad (9)$$

During the adaptive k-integration, these terms must be evaluated at arbitrary k-points not necessarily contained in the k-mesh used for the Wannier projection. As we will see establishing connection between the Bloch and Wannier states at the extra k-points poses some challenges.

But first, the Bloch-only term,

$$\mathcal{T}_{\psi\psi} = A_{ii}(\omega) V_{ij}^\alpha A_{jj}(\omega + \Omega) V_{ji}^\beta, \quad (10)$$

simplifies because the matrix spectral function is diagonal. It can be computed using the noninteracting formula

$$A_{ii}(\mathbf{k}, \omega) = \frac{2\delta/\tau}{(\omega - \varepsilon_i(\mathbf{k}) + \mu)^2 + \delta^2}, \quad (11)$$

where δ is a broadening parameter (corresponding to a self-energy $\Sigma = -i\delta$ with a small $\delta > 0$). The momentum matrix elements V_{ij}^α are taken directly from WIEN2k's optic module [AS06].

Next, for the Wannier-only part,

$$\mathcal{T}_{ww} = A_{uv}(\omega) V_{vr}^\alpha A_{rs}(\omega + \Omega) V_{su}^\beta, \quad (12)$$

we have to mediate between the spectral function, which will be given in the Wannier gauge in terms of the DMFT self-energy $\Sigma(\omega)$ via the Green function

$$G(\mathbf{k}, \omega) = [\omega - H^W(\mathbf{k}) + \mu - \Sigma(\omega)]^{-1}; \quad (13)$$

and the momentum matrix elements, which `optic` computes in the Kohn-Sham (ks) gauge. In our index convention,

$$V_{uv}^\alpha(\mathbf{k}) = \langle w u k | \hat{p}_\alpha | w v k \rangle = \mathcal{U}_{un}^+(\mathbf{k}) V_{nm}^\alpha(\mathbf{k}) \mathcal{U}_{mv}(\mathbf{k}). \quad (14)$$

But if \mathbf{q} is a new k-point not included in the original Wannier mesh \mathcal{W} , $\mathcal{U}(\mathbf{q})$ is unknown. To determine \mathcal{U} for new k-points, Wannier interpolation [Mar+12; Yat+07] can be used in the following way [Wis12]: For each new k-point $\mathbf{q} \notin \mathcal{W}$, the Wannier Hamiltonian

$$H_{uv}^W(\mathbf{k}) = \langle w u k | \hat{H}_{\text{KS}} | w v k \rangle = \mathcal{U}_{un}^+(\mathbf{k}) \varepsilon_n(\mathbf{k}) \mathcal{U}_{nv}(\mathbf{k}) \quad (15)$$

is interpolated to $H^W(\mathbf{q})$, and the unitary matrix $\tilde{\mathcal{U}}(\mathbf{q})$ which diagonalizes it is taken as $\mathcal{U}(\mathbf{q})$.

With $V_{nm}^\alpha(\mathbf{q})$ calculated by `optic` and $\Sigma(\omega)$ k-independent, all the ingredients are at hand to calculate \mathcal{T}_{ww} at \mathbf{q} . This is the approach used in the original `WOPTIC` implementation [Wis12]. It is straightforwardly generalized to the mixed term

$$\mathcal{T}_{w\psi} = A_{uv}(\omega) V_{vi}^\alpha A_{ii}(\omega + \Omega) V_{iu}^\beta + A_{ii}(\omega) V_{iu}^\alpha A_{uv}(\omega + \Omega) V_{vi}^\beta. \quad (16)$$

However, there is a subtler problem. Since the $|\psi ak\rangle$ arise from the diagonalization of $\hat{H}_{\text{KS}}(\mathbf{k})$, they carry complex phases $\varphi_a(\mathbf{k})$ which a priori are completely arbitrary. On the original k-points $\mathbf{k} \in \mathcal{W}$, the $\mathcal{U}(\mathbf{k})$ take into account and “cancel” these phases, yielding smooth functions $|w v k\rangle = \mathcal{U}_{iv}(\mathbf{k}) |\psi ik\rangle$ of \mathbf{k} ; but on added k-points $\mathbf{q} \notin \mathcal{W}$, $\tilde{\mathcal{U}}(\mathbf{q})$ has no such constraint, and the phases enter into $\mathcal{T}_{w\psi}$ and \mathcal{T}_{ww} via the momentum matrix elements. (In $\mathcal{T}_{\psi\psi}$ the phases cancel because V_{ij}^α always appears paired with V_{ji}^β .)

2.1 Wannier-interpolating the momentum matrix elements

The solution to this “random-phase problem”* explored in the present work is a direct Wannier interpolation of $V^\alpha(k)$. That is, $V_{nm}^\alpha(k)$ is computed by optic on $k \in \mathcal{W}$ and transformed to the Wannier gauge (14). For all new k-points q , $V_{uv}^\alpha(q)$ can be computed via Fourier interpolation,

$$V_{uv}^\alpha(q) = \frac{1}{|\mathcal{W}|} \sum_{R \in \mathcal{W}} e^{iRq} V_{uv}^\alpha(R). \quad (17)$$

Then, \mathcal{T}_{WW} can be computed completely in the Wannier gauge without recourse to any new $\tilde{\mathcal{U}}(q)$.

For this strategy to work,

$$V_{uv}^\alpha(R) = \langle w u 0 | \hat{p}_\alpha | w v R \rangle \quad (18)$$

must be well-localized in direct space, which should be the case as long as well-localized wf can be found. This approach has been tested numerically for the case of SrVO₃.

First, the rapid decay of $V_{uv}^\alpha(R)$ with $|R|$ is seen in Fig. 4. With exponentially localized wf, we expect exponential decay $\sim e^{-|R|}$, consistent with the apparent linear behavior in the semilogarithmic plot. Second, as long as the wf are real, $V_{uv}^\alpha = \langle w u k | -i\partial_\alpha | w v k \rangle$ should be purely imaginary, as confirmed numerically in Fig. 5. Third, the Peierls approximation suggests that $V(R) \approx RH^w(R)$, as shown in Fig. 6.

These results already make a strong case for the Wannier interpolation method as applied to \mathcal{T}_{WW} . In Sec. 3 we will see that this is validated also in the k-integrated optical conductivity.

2.2 Interpolating the mixed momentum matrix elements

The mixed matrix elements $V_{vi}^\alpha = \langle w v k | \hat{p}_\alpha | \psi i k \rangle$ are not amenable to interpolation in the same way as $V_{uv}^\alpha(R)$ because $V_{vi}^\alpha(R)$ does not decay with $|R|$ (it does not in numerical tests, and neither is there much reason to believe it

* In crystal structures with inversion symmetry, it is a well-known and computationally exploited fact that the ks vectors (more properly their basis coefficients and the necessary matrix elements) can be chosen to be real. It is tempting to conclude that there is no random-phase problem in these cases; however, the freedom to choose an arbitrary sign at each k-point, $\varphi(k) \in \{0, \pi/2\}$, remains.

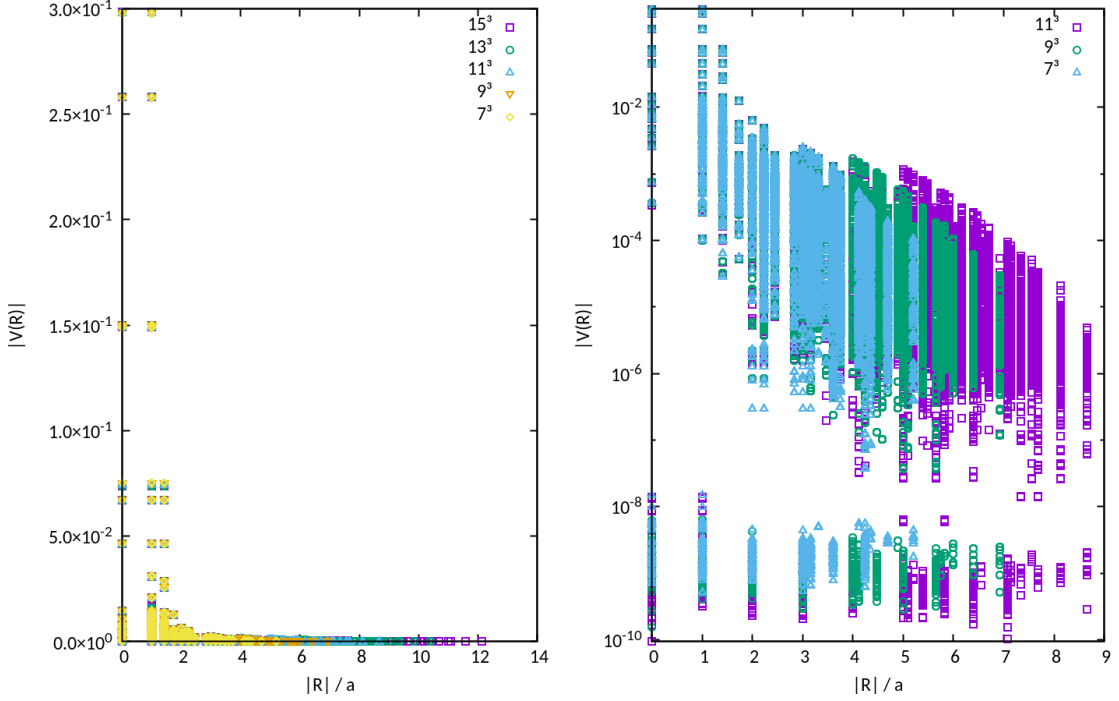


Figure 4: $|V_{uv}^\alpha(\mathbf{R})|$ for SrVO_3 as a function of $|\mathbf{R}|$ in units of the lattice constant. The Wannier projection spans the O-p and V-d bands (P-14 above), and different Wannierization k-meshes are compared. For each k-mesh, all the matrix elements (for all values of u , v , and \mathbf{R}) are plotted together. Denser meshes in reciprocal space correspond to larger supercells in direct space, therefore they show a greater range and density of $|\mathbf{R}|$ values. The linear plot (left) shows that the matrix elements are well converged already at 7^3 k-points. In the semilogarithmic plot (right), the separation between signal and numeric noise becomes evident. The magnitude of the noise decreases as the k-mesh density increases. The signal roughly follows a straight line, consistent with exponential localization.

should). Since the matrix elements appear in the trace in terms of the form $V_{ui}^\alpha A_{ii}(\omega) V_{iv}^\beta A_{vu}(\omega + \Omega)$, two alternative targets for interpolation present themselves:

$$S_{uiv}^{\alpha\beta}(\mathbf{k}) := V_{ui}^\alpha \cdot V_{iv}^\beta = \langle w u \mathbf{k} | \hat{p}_\alpha | \psi i \mathbf{k} \rangle \langle \psi i \mathbf{k} | \hat{p}_\beta | w v \mathbf{k} \rangle \quad (19)$$

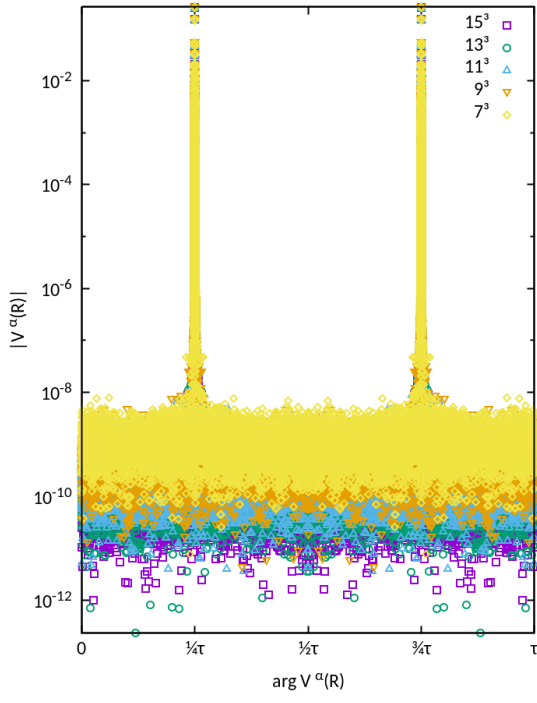


Figure 5: $|V_{uv}^\alpha(\mathbf{R})|$ as a function of the complex argument $\varphi = \arg V_{uv}^\alpha(\mathbf{R})$. (Same data as Fig. 4.) As expected for real-valued wf, $V_{uv}^\alpha(\mathbf{R})$ is purely imaginary, except for the numerical noise which has uniformly distributed phases.

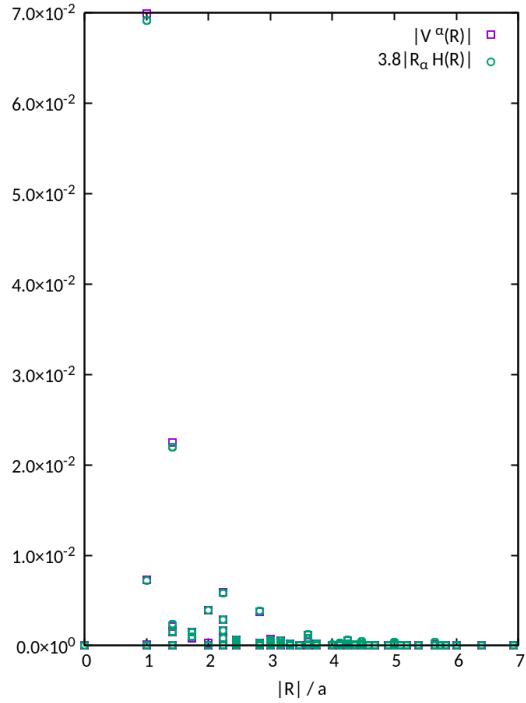


Figure 6: $|V_{uv}^\alpha(\mathbf{R})|$ compared to the Peierls expression $|\mathbf{R}H_{uv}^W(\mathbf{R})|$ (times a fitted constant) as a function of $|\mathbf{R}|$. In this case, a 3-band Wannier projection on $9 \times 9 \times 9$ k-points encompassing only the V-t_{2g} bands (p-3 above) was used, otherwise the positions of the wf within the unit cell would have to be taken into account in the Peierls approximation.

(no summation implied) or

$$\begin{aligned} W_{uv}^{\alpha\beta}(\mathbf{k}, \omega) &:= V_{ui}^\alpha A_{ii}(\mathbf{k}, \omega) V_{iv}^\beta \\ &= \langle \text{w } u\mathbf{k} | \hat{p}_\alpha \left(\sum_i |\psi i\mathbf{k}\rangle A_{ii}(\mathbf{k}, \omega) \langle \psi i\mathbf{k}| \right) \hat{p}_\beta | \text{w } v\mathbf{k} \rangle; \end{aligned} \quad (20)$$

in each case at the cost of dealing with a larger, more complicated, object. Numerically, $S_{uv}^{\alpha\beta}(\mathbf{R})$ does not show decay with $|\mathbf{R}|$, and we therefore discard this approach.

There is some justification to expect

$$W_{uv}^{\alpha\beta}(\mathbf{R}, \omega) = \frac{V_{\text{UC}}}{\tau^3} \int_{\text{BZ}} d\mathbf{k} e^{-i\mathbf{k}\mathbf{R}} W_{uv}^{\alpha\beta}(\mathbf{k}, \omega) \quad (21)$$

to do better (the unit cell volume V_{UC} enters through the normalization of the Fourier transform). Denoting the operator $\hat{p}_\alpha(\dots)\hat{p}_\beta$ above as $\hat{B}(\mathbf{k})$ and suppressing the ω -dependence, we can write the Fourier transform as a convolution

$$W_{uv}^{\alpha\beta}(\mathbf{R}) = \sum_{\mathbf{R}'\mathbf{R}''} \langle \text{w } u\mathbf{R}' | \hat{B}(\mathbf{R} + \mathbf{R}' - \mathbf{R}'') | \text{w } v\mathbf{R}'' \rangle. \quad (22)$$

Thus, the properties of $\hat{B}(\mathbf{R})$ determine the degree of localization of $W_{uv}^{\alpha\beta}(\mathbf{R})$.

To arrive at an expression analogous to (18), we must suppose that $\hat{B}(\mathbf{k})$ is \mathbf{k} -independent, and thus $\hat{B}(\mathbf{R}) = \delta_{\mathbf{R},0}\hat{B}$, which yields

$$W_{uv}^{\alpha\beta}(\mathbf{R}) = \sum_{\mathbf{R}'} \langle \text{w } u\mathbf{R}' | \hat{B} | \text{w } v\mathbf{R} + \mathbf{R}' \rangle. \quad (23)$$

In this case it is clear that $W_{uv}^{\alpha\beta}$ will be localized in terms of \mathbf{R} as long as \hat{B} is a sufficiently local operator (i.e., $\langle \mathbf{r}' | \hat{B} | \mathbf{r}'' \rangle$ is localized in terms of $|\mathbf{r}' - \mathbf{r}''|$). If furthermore $\hat{B}(\mathbf{R})$ is lattice-translation invariant (meaning that $\langle \mathbf{r}' - \mathbf{R} | \hat{B}(\mathbf{R}) | \mathbf{r}'' - \mathbf{R} \rangle \equiv \langle \mathbf{r}' | \hat{B}(\mathbf{R}) | \mathbf{r}'' \rangle$), we find, as desired,

$$W_{uv}^{\alpha\beta}(\mathbf{R}) = \langle \text{w } u\mathbf{0} | \hat{B} | \text{w } v\mathbf{R} \rangle. \quad (24)$$

Considering the actual form of \hat{B} (20), to get the simple case (24), we have to assume that (a) the Bloch states i are “nearly complete”, and (b) $A_{ii}(\mathbf{k}, \omega) \approx A(\omega)$ is nearly constant in i and \mathbf{k} . In this case,

$$\sum_i |\psi i\mathbf{k}\rangle A_{ii}(\omega) \langle \psi i\mathbf{k}| \approx A(\omega) \hat{P}(\mathbf{k}), \quad (25)$$

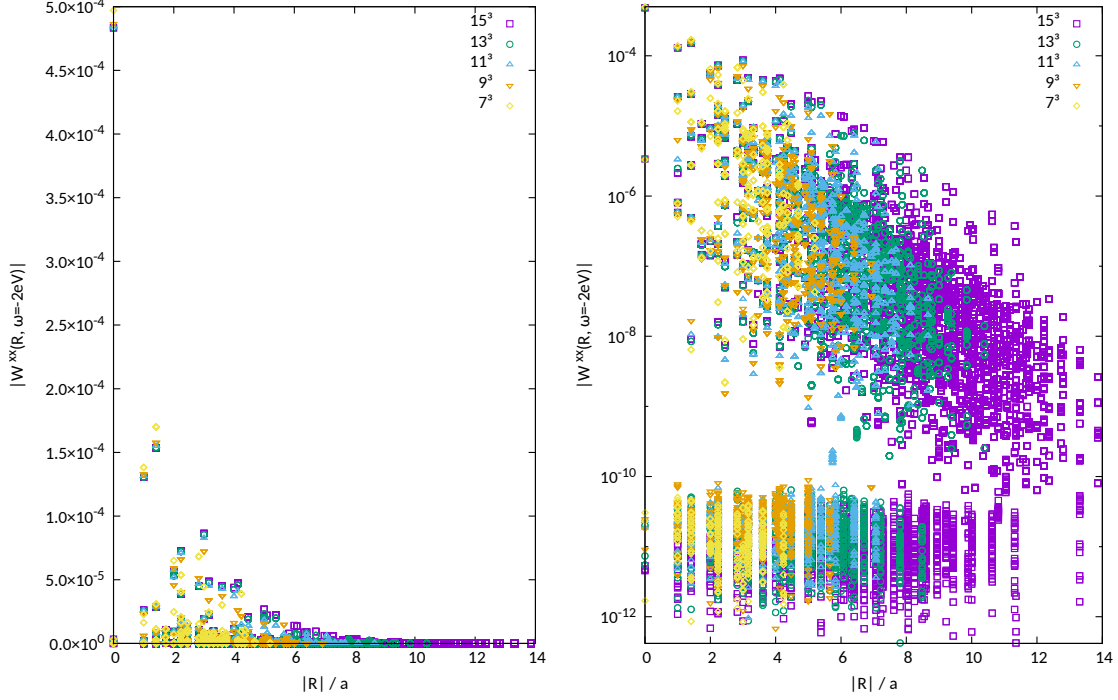


Figure 7: Like Fig. 4, but for the mixed matrix elements $W_{uv}^{\alpha\alpha}(\mathbf{R}, \omega = -2 \text{ eV})$ instead of $V_{uv}^{\alpha}(\mathbf{R})$. At this frequency, a satisfactory (apparently exponential) decay with $|\mathbf{R}|$ is seen, albeit slower than for $|V^{\alpha}(\mathbf{R})|$. The Wannier projections are on the V-t_{2g} bands (p-3 above), as in Fig. 6, and the outer (“Bloch”) window spans the O-p and V-e_g bands.

where $\hat{P}(\mathbf{k})$ is the projector onto \mathbf{k} and can be replaced by $\hat{\mathbb{1}} = \int d\mathbf{k} \hat{P}(\mathbf{k})$ since $\langle \psi i\mathbf{k} | \hat{p}_{\alpha} | w u\mathbf{k}' \rangle$ enforces $\mathbf{k} = \mathbf{k}'$ anyway. This yields

$$W_{uv}^{\alpha\beta}(\mathbf{R}, \omega) \approx A(\omega) \langle w u \mathbf{0} | \hat{p}_{\alpha} \hat{p}_{\beta} | w v \mathbf{R} \rangle. \quad (26)$$

However, it is difficult to see how these conditions would be satisfied in a real calculation; (a) means that $\langle w u \mathbf{k} | \hat{p}_{\alpha} | w v \mathbf{k} \rangle \approx 0$, i.e. no w-w transitions are allowed,* and (b) is only the case in energy regions without Bloch states, where $A_{ii} = W_{uv}^{\alpha\beta} = 0$. Otherwise the noninteracting spectral function is in fact a sum over δ -peaks, $A_{ii}(\mathbf{k}) = \sum_j w_j^{(i)} \delta(\mathbf{k} - \mathbf{x}_j^{(i)})$.

Numerical tests for $W_{uv}^{\alpha\beta}(\mathbf{R}, \omega)$ analogous to those for V_{uv}^{α} conclude this section (Figs. 7 to 10). In this case the analysis is complicated by the extra dependence

* Strictly speaking, the requirement is $\sum_{rs} \langle w u \mathbf{k} | \hat{p}_{\alpha} | w r \mathbf{k} \rangle \langle w s \mathbf{k} | \hat{p}_{\beta} | w v \mathbf{k} \rangle \approx 0$.

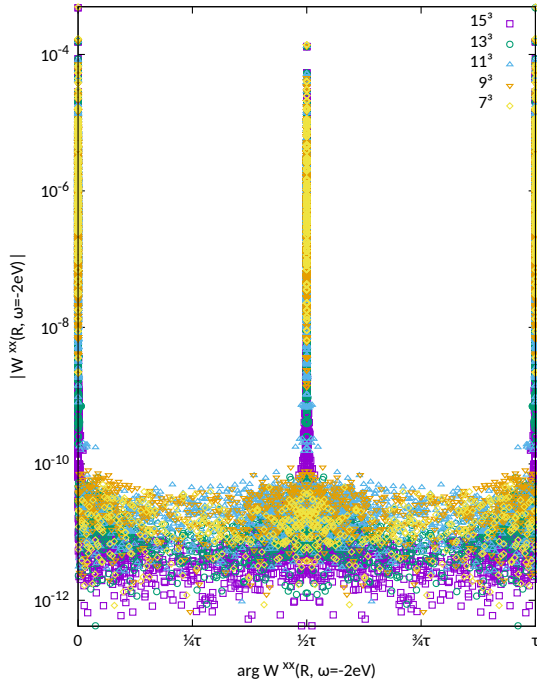


Figure 8: As Fig. 5, but for the mixed matrix elements $W_{uv}^{\alpha\alpha}(R, \omega = -2 \text{ eV})$ instead of $V_{uv}^\alpha(R)$. (Same data as Fig. 7.) A similar picture emerges for $W^{\alpha\neq\beta}$ (not shown).

on ω , which turns out to be important, and the fact that $W^{\alpha\beta}$ carries two coordinate indices instead of one. Overall, $W_{uv}^{\alpha\beta}(R, \omega)$ shows significant localization. Furthermore, it is essentially real, as we would expect in the simple scenario of (26). The latter observation holds even where $W_{uv}^{\alpha\beta}(R, \omega)$ is not well localized. In the face of the considerations above, both the localization and realness of $W_{uv}^{\alpha\beta}(R)$ are surprising, and an explanation remains as a topic for future study. Results for the optical conductivity will be shown in Sec. 3. In this case as well, we will see that the interpolation works acceptably well overall.

To begin, let $\alpha = \beta$ and the internal frequency $\omega = -2 \text{ eV}$, where $W_{uv}^{\alpha\alpha}(R, \omega)$ is comparatively well behaved (Fig. 7). This corresponds to the top of the O-p bands. Fig. 8 shows that $W_{uv}^{\alpha\alpha}$ is essentially real. The situation is largely the same for $\alpha \neq \beta$ (the off-diagonal terms of the optical conductivity), including the magnitude of $W_{uv}^{\alpha\neq\beta}$, even though these contributions must integrate to 0 in $\sigma^{\alpha\beta}(\omega)$ for this cubic material (Fig. 9).

At $\omega = -4.5 \text{ eV}$ (Fig. 10), corresponding to the center of the O-p bands, there is still some decay, but it is not as pronounced. Note also that this coincides with larger magnitudes of $W_{uv}^{\alpha\beta}$. The realness of $W_{uv}^{\alpha\beta}(R)$ remains untouched by

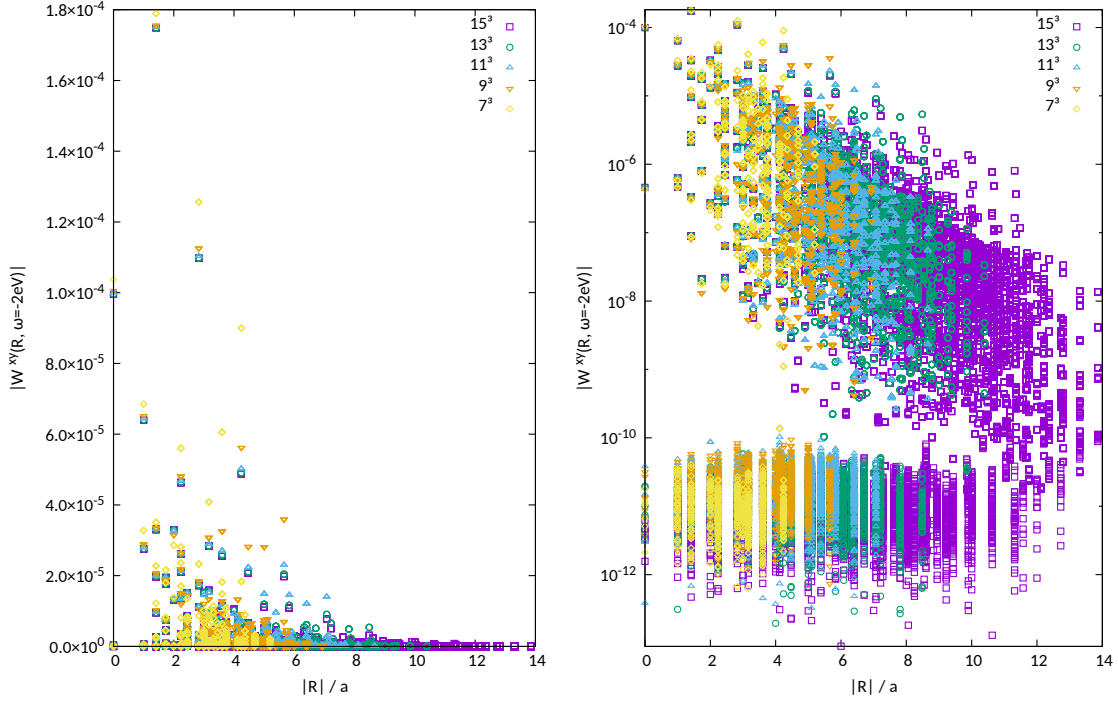


Figure 9: Like Fig. 7, but off-diagonal in the Cartesian indices, $\alpha \neq \beta$.

this change (the phase plot as in Fig. 8 is similar at both frequencies, and hence not shown for $\omega = -4.5$ eV).

2.3 Interpolation and disentanglement

In the above description, it was implicit that the WF were constructed without disentanglement. The basic difficulty was that we needed to mediate between the “Bloch” and “Wannier” bases at k -points q where $\mathcal{U}(q)$ is not available. This problem is addressed in WOPTIC by interpolating either the transformation matrices $\tilde{\mathcal{U}}(q)$, or the momentum matrix elements V^α , $W^{\alpha,\beta}$.

In the presence of disentanglement, we face a similar problem concerning the projector matrices $\mathcal{V}(k)$ to the optimal subspace. Recall that the $\mathcal{V}(k)$ have dimension $\mathcal{J}_k \times J$, where J is the number of wf and \mathcal{J}_k the number of bands at k , and satisfy

$$\mathcal{V}^+(k)\mathcal{V}(k) = \mathbb{1}_{J \times J}. \quad (27)$$

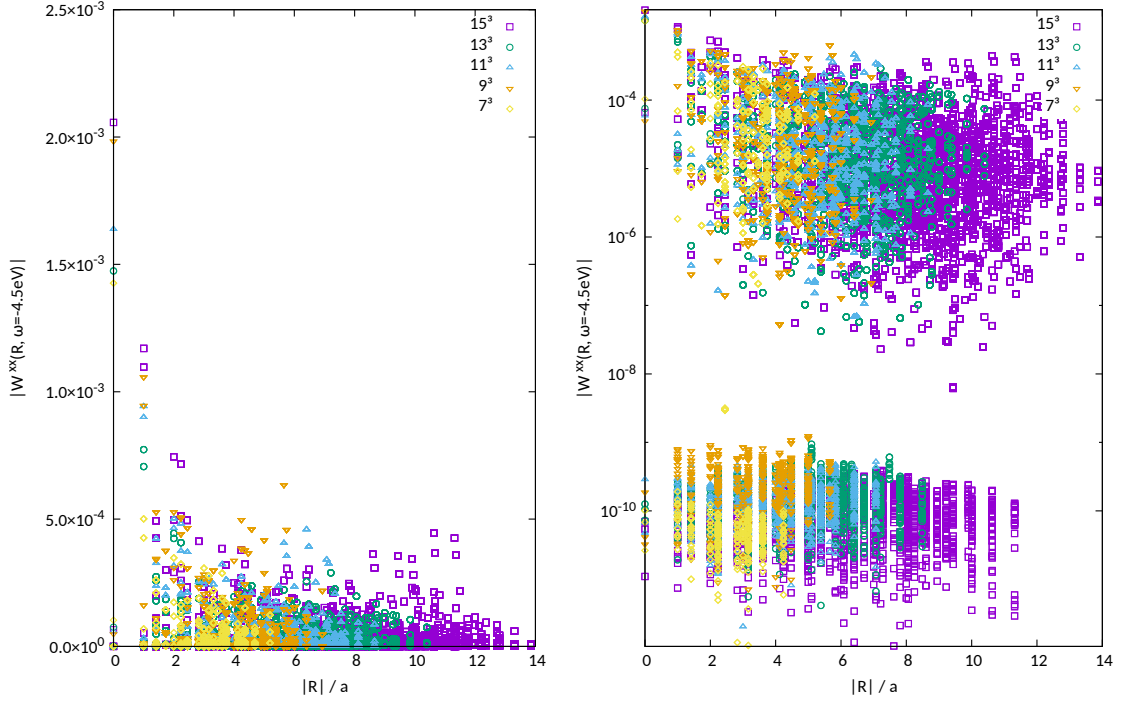


Figure 10: Like Fig. 7, at internal frequency $\omega = -4.5$ eV. Even though the localization is lacking in this case, $W^{\alpha\beta}$ is still essentially real-valued.

This section will explore strategies to overcome this obstacle. However, the current version of wOPTIC supports only the simplest special case including disentanglement, namely when only w-w transitions are included, and those are treated using Wannier interpolation.

General considerations

Disentanglement does not change the general structure of the problem. It is still useful to partition the Hilbert space into inner and outer parts. This time, the inner subspace will encompass all states that participate in the disentanglement; it is what happens inside this part that becomes more complicated. For the purposes of this discussion, upper case letters H, Σ, G, A refer to quantities in the whole “Wannier+Bloch” space (the physical quantities, as it were); lower case letters ε, g, a refer to their parts within or without the disentanglement window; a superscript w indicates a quantity in the Wannier basis (with the disentangled

states projected out); and a superscript \star indicates the same quantity promoted to the whole disentanglement subspace (i.e., $\cdot^\star = \mathcal{V}\mathcal{U} \cdot \mathcal{U}^+\mathcal{V}^+$, going from a $\mathcal{J}_k \times \mathcal{J}_k$ to a $J \times J$ matrix).

Let us write the diagonal ks Hamiltonian as

$$H = \begin{pmatrix} \varepsilon' & & \\ & \varepsilon & \\ & & \varepsilon'' \end{pmatrix}, \quad (28)$$

where ε is the inner part of dimension $\mathcal{J}_k \times \mathcal{J}_k$, and the outer part is made up of ε' and ε'' . In order to introduce the $J \times J$ single-particle Hamiltonian used in the many-body calculation,

$$H_{uv}^W = \mathcal{U}_{un}^+ \mathcal{V}_{na}^+ \varepsilon_a \mathcal{V}_{am} \mathcal{U}_{mv}, \quad (29)$$

into (28), we use the $(\mathcal{J}_k \times \mathcal{J}_k)$ projector onto the optimal subspace and its complement within the disentanglement window,

$$P = \mathcal{V}\mathcal{V}^+ \quad \text{and} \quad Q = \mathbb{1} - P, \quad (30)$$

to write

$$\varepsilon = P\varepsilon P + Q\varepsilon Q + P\varepsilon Q + Q\varepsilon P, \quad (31)$$

where

$$P\varepsilon P = \mathcal{V}\mathcal{U}H^W\mathcal{U}^+\mathcal{V}^+ = H^* \quad (32)$$

corresponds to H^W promoted to $(\mathcal{J}_k \times \mathcal{J}_k)$.

We must now calculate the spectral function. The Green function

$$G = (\omega - H - \Sigma)^{-1} = \begin{pmatrix} g'_0 & & \\ & g & \\ & & g''_0 \end{pmatrix} \quad (33)$$

inherits the block-diagonal form of the Hamiltonian, as does the spectral function

$$A = \frac{i}{\tau}(G - G^+) = \begin{pmatrix} a'_0 & & \\ & a & \\ & & a''_0 \end{pmatrix}, \quad (34)$$

where g_0 and a_0 stand for the noninteracting Green function and spectral function (11) outside of the disentanglement window.

In constructing the Green function, the self-energy $\Sigma^w (J \times J)$ derived from the many-body calculation should be applied only to the Wannier (P) part of the states. It must be promoted to $\Sigma^* (\mathcal{J}_k \times \mathcal{J}_k)$. For computational purposes, a finite broadening ($\Sigma \leftarrow -i\delta$) will be imposed on all other states (Q , as well as outside the disentanglement window).

Thus, the inverse of the inner-window Green function is

$$\begin{aligned} g^{-1} &= \omega \mathbb{1}_{\mathcal{J}_k} - \varepsilon - \Sigma^* + i\delta Q \\ &= \mathcal{V}\mathcal{U}(\omega \mathbb{1}_J - H^w - \Sigma^w)\mathcal{U}^+\mathcal{V}^+ + (\omega + i\delta)Q - (\varepsilon - P\varepsilon P) \end{aligned} \quad (35)$$

(since for a projector Q and a scalar c , $Qc\mathbb{1}Q = cQ$). But due to the inversion, neither the Green function itself nor the spectral function

$$a = -\frac{i}{\tau}(g - g^+) \quad (36)$$

admits a similar partitioning. Evidently, in the disentangled case, both $\mathcal{U}(\mathbf{q})$ and $\mathcal{V}(\mathbf{q})$ are needed on the new k-points. Wannier interpolation of the momentum matrix elements is not applicable.

Wannier-Wannier transitions only

Consider now the special case mentioned above, where we are interested only in w-w transitions but disentanglement is necessary, e.g., to remove extraneous states that interfere with the target states at the band edges, as in the P-14 for SrVO₃. Under these circumstances, Wannier interpolation can be salvaged in the presence of disentanglement.

Namely, we can work entirely in the Wannier basis, where

$$G^w = (\omega \mathbb{1}_J - H^w - \Sigma^w)^{-1} \quad (37)$$

and

$$\mathcal{T} = \mathcal{T}_{ww} = \text{tr } A^w(\omega) \mathcal{V}^+ \mathcal{U}^+ V^\alpha \mathcal{U} \mathcal{V} A^w(\omega + \Omega) \mathcal{V}^+ \mathcal{U}^+ V^\beta \mathcal{U} \mathcal{V}; \quad (38)$$

$\mathcal{V}^+ \mathcal{U}^+ V^\alpha \mathcal{U} \mathcal{V} = (V^\alpha)^w$ can be identified as the momentum matrix elements in the Wannier basis and subjected to Wannier interpolation.

Interpolating $\mathcal{V}(k)$

The interpolation method for $\tilde{\mathcal{U}}(\mathbf{q})$ cannot be extended to the rectangular $\mathcal{V}(\mathbf{q}) (\mathcal{J}_q \times J)$, even disregarding any random-phase problem. To obtain interpolated $\tilde{\mathcal{V}}$, it seems most promising to extend the computational definition

of $\mathcal{V}(\mathbf{k})$. The $|\tilde{\psi} \ nk\rangle$ are computed as the eigenvectors corresponding to the J largest eigenvalues of the $\mathcal{J}_k \times \mathcal{J}_k$ matrix $Z(\mathbf{k})$ with elements [Mar+12, Eq. (53)]

$$Z_{mn} := \langle \mathbf{u} \ m\mathbf{k} | \sum_b g_b P_{\mathbf{k}+\mathbf{b}} | \mathbf{u} \ n\mathbf{k} \rangle. \quad (39)$$

The projector $P_k = \sum_r |\tilde{\psi} \ rk\rangle \langle \tilde{\psi} \ rk| \hat{=} \mathcal{V}(\mathbf{k}) \mathcal{V}^+(\mathbf{k})$ onto the optimal subspace is the same as above. In the course of the normal disentanglement routine, this equation is iterated, using the projector from the previous iteration to compute the next Z until P and Z are consistent with each other.

If the optimally smooth subspace is known on a sufficiently fine \mathbf{k} -mesh, (39) can be reinterpreted to provide interpolated $\tilde{\mathcal{V}}$. Let $\mathbf{q} \notin \mathcal{W}$ be a new \mathbf{k} -point, and \mathbf{b} point to its neighbors on the original \mathbf{k} -mesh, $\mathbf{q} + \mathbf{b} \in \mathcal{W}$. Now we can keep $P_{\mathbf{q}+\mathbf{b}}$ fixed and use it as a boundary condition to compute $Z(\mathbf{q})$ and hence $\tilde{\mathcal{V}}(\mathbf{q})$.

Recall that the sum over \mathbf{b} and weights $g_{\mathbf{b}}$ stem from the finite-difference formulas [Mos+08, Eqs. (8) and (9)]

$$\nabla f(\mathbf{k}) = \sum_{\mathbf{b}} g_{\mathbf{b}} \mathbf{b} [f(\mathbf{k} + \mathbf{b}) - f(\mathbf{k})] + \mathcal{O}(b^2), \quad (40)$$

$$|\nabla f(\mathbf{k})|^2 = \sum_{\mathbf{b}} g_{\mathbf{b}} [f(\mathbf{k} + \mathbf{b}) - f(\mathbf{k})]^2 + \mathcal{O}(b^3), \quad (41)$$

where b is the \mathbf{k} -mesh spacing. These expressions are valid under the condition that [Mos+08, Eq. (26)]

$$\sum_{\mathbf{b}} g_{\mathbf{b}} b_{\alpha} b_{\beta} = \delta_{\alpha\beta}. \quad (42)$$

Wannier90 ensures this in the following way: Add shells of neighbors with increasing $|\mathbf{b}|$. Compute the N_b weights by interpreting (42) as a linear system of equations and solving for $g_{\mathbf{b}}$. Stop when (42) is satisfied.*

This procedure is applicable with little or no change also for an arbitrary point \mathbf{q} , and so it should be possible to construct interpolated $\tilde{\mathcal{V}}(\mathbf{q})$; however, the random-phase problem will apply here, as well.

* For the linear system of equations to be solvable, it is sufficient but not necessary to have 6 linearly independent \mathbf{b} vectors.

3 Numerical results for the optical conductivity

The tests on the momentum matrix elements $V^\alpha(\mathbf{R})$ and $W^{\alpha\beta}(\mathbf{R}, \omega)$ presented in the preceding section are insightful precisely because they address the interpolated quantities directly. However, we have yet to address the bottom line: how the observable, k-integrated, quantities are affected. The random-phase problem in the case of \mathcal{U} interpolation in particular can only be quantified in this way. In this section, optical conductivities (including the dc conductivity as the $\Omega \rightarrow 0$ limit) computed using the different approaches will be compared. SrVO₃ will be used as a testbed material throughout. A noninteracting model and other limiting cases where certain sources of error are known to be absent provide a basis for the analysis.

Unless noted otherwise, the Wannier projections were made on a $9 \times 9 \times 9$ k-mesh, consequently $V^\alpha(\mathbf{R})$ and $W^{\alpha\beta}(\mathbf{R}, \omega)$ were constructed on a $9 \times 9 \times 9$ supercell. This size was chosen so that the quantities in the Wannier gauge are relatively well converged, while the computational effort remains manageable. In particular, the Wannier Hamiltonian is well converged on this mesh, as is $V^\alpha(\mathbf{R})$ (cf. Fig. 6). $W^{\alpha\beta}(\mathbf{R}, \omega)$ is reasonably well converged at favorable frequencies (cf. Fig. 7) but perhaps less so at unfavorable ones (cf. Fig. 10). All results are converged with respect to the integration k-mesh.

3.1 Noninteracting models

The noninteracting optical conductivity is an important test case, where “non-interacting” means that only a small imaginary self-energy is added to the WIEN2k bands for broadening, $\Sigma \leftarrow -i\delta$. On the one hand, the random-phase problem in the \mathcal{U} interpolation approach is absent (by the same argument as for the $\mathcal{T}_{\psi\psi}$ term in (9), i.e., that the matrix spectral function is diagonal in the Bloch basis). On the other hand, the WOPTIC results can be directly compared to WIEN2k’s optic module.

Adaptively integrated results

Fig. 11 shows a comparison of the WIEN2k result to four variants of WOPTIC, which ideally should all be identical:

- (N1) WIEN2k optic — black line and shaded,

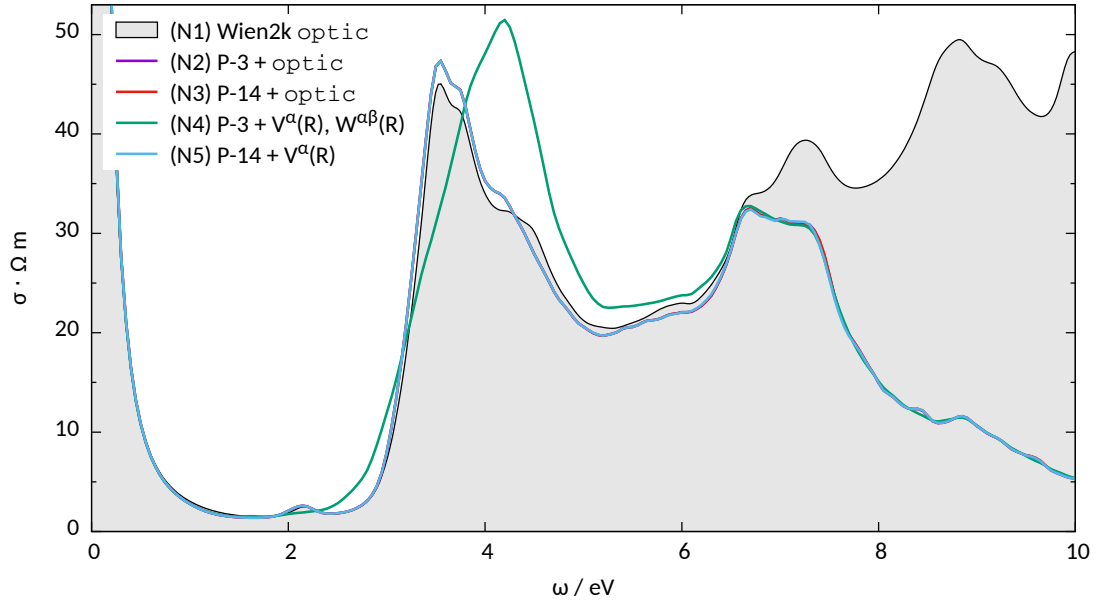


Figure 11: Noninteracting optical conductivity computed by WIEN2k's `optic` compared with different variants of `WOPTIC`. See text for details.

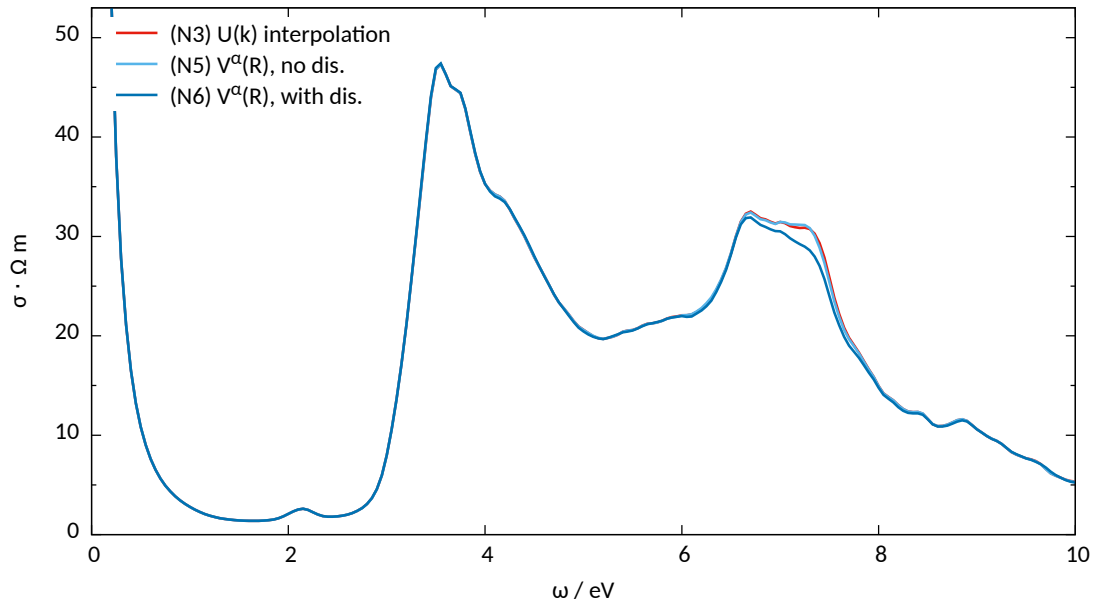


Figure 12: Noninteracting optical conductivity computed from p-14 projections with and without disentanglement. See text for details.

- (N2) P-3 projection with interpolated $\mathcal{U}(\mathbf{k})$ and matrix elements from `optic` — purple line,
- (N3) P-14 projection with interpolated $\mathcal{U}(\mathbf{k})$ and matrix elements from `optic` — red line,
- (N4) P-3 projection with interpolated momentum matrix elements $V^\alpha, W^{\alpha\beta}$ — green line,
- (N5) P-14 projection with interpolated momentum matrix elements V^α — blue line.

Note that each `WOPTIC` calculation takes into account the same 14 bands (O-p and V-d); P-14 includes all of them as `wf` (i.e. there are only w-w transitions in (N3) and (N5)), while P-3 includes only the V-t_{2g} states as `wf`, and the other states in the form of ψ - ψ and w- ψ transitions.

As a first observation, there is reasonable agreement between `optic` (N1) and the `WOPTIC` curves (N2), (N3), and (N5). Up to frequencies ~ 4 eV, the curves match well; for larger frequencies, deviations are expected because transitions outside of the `WOPTIC` window become relevant. The comparison of `WOPTIC` to `optic` has already been addressed previously [Ass+15; Wis12]; the remaining differences can be attributed to temperature (the `WOPTIC` calculations were done at $\beta = 40 \text{ eV}^{-1}$ while `optic` works in the ground state) and the different broadening schemes. In any case, the focus here is on the relative performance of the momentum matrix element interpolation and $\mathcal{U}(\mathbf{k})$ interpolation.

Moreover, curves (N2), (N3), and (N5) are almost identical. This shows that Wannier interpolation for the w-w transitions works well, and that the different Wannier projections introduce no change in the optical conductivity. (Recall that the *raison d'être* of the V^α and $W^{\alpha\beta}$ interpolation, the random phase problem, is absent in this noninteracting case.)

Conversely, curve (N4) clearly shows interpolation errors in the region where w- ψ transitions are important (approximately 2 to 6 eV). We will have a closer look at these errors in Fig. 13.

But first, to test the procedure for disentanglement taking into account w-w transitions only as outlined in Sec. 2.3. Fig. 12 adds another:

- (N6) P-14 with disentanglement and interpolated momentum matrix elements V^α — dark blue line.

The agreement of this curve with the others is within reasonable expectations. The differences introduced by disentanglement are small and mostly contained in a narrow region around $\omega \approx 7$ eV, corresponding to transitions around the R-point (the only region where disentanglement is active, cf. Fig. 3). Since the models with and without disentanglement represent slightly different physics, they cannot be expected to yield identical results.

Contributions by subspace

The curves shown in Fig. 11 were calculated by converging WOPTIC on an adaptive k-mesh. This has the advantage that it corresponds to the intended usage of the code; the disadvantage is that, if there is disagreement between the different modes, the adaptively refined k-meshes will likewise be different, which could distort the intrinsic differences. Therefore, Fig. 13 shows the noninteracting optical conductivity obtained with uniform refinement, separated into w-w, w- ψ , and $\psi-\psi$ contributions. For each contribution, two curves are shown, corresponding to (N2) and (N4) above. The logarithmic scale serves to show all the contributions in one plot, but since it may obscure the magnitude of disagreement between the curves. the relative errors between the two approaches are shown in a lower panel. Fig. 13 confirms that the divergence of (N4) from the other curves in Fig. 11 is due to the w- ψ contribution. In particular, we see that both the peak at $\omega \approx 2$ eV which (N4) misses almost entirely, and the second, larger peak at $\omega \approx 4$ eV, which is shifted and distorted in (N4), are dominated by mixed transitions.

3.2 Interacting models

A nontrivial self-energy $\Sigma(\omega)$ will now be added. The self-energy (shown in Fig. 14) is taken from a DMFT calculation using a 3-band model for SrVO₃ [Ass+15; Wis12]. For testing purposes it will also be applied to the d-orbitals of the P-14 projections, even though this is unphysical. To discuss the different WOPTIC variants, let us use the following labels in analogy to the noninteracting case:

- (I2) P-3 model with interpolated $\mathcal{U}(k)$ and matrix elements from optic
- (I3) P-14 model with interpolated $\mathcal{U}(k)$ and matrix elements from optic

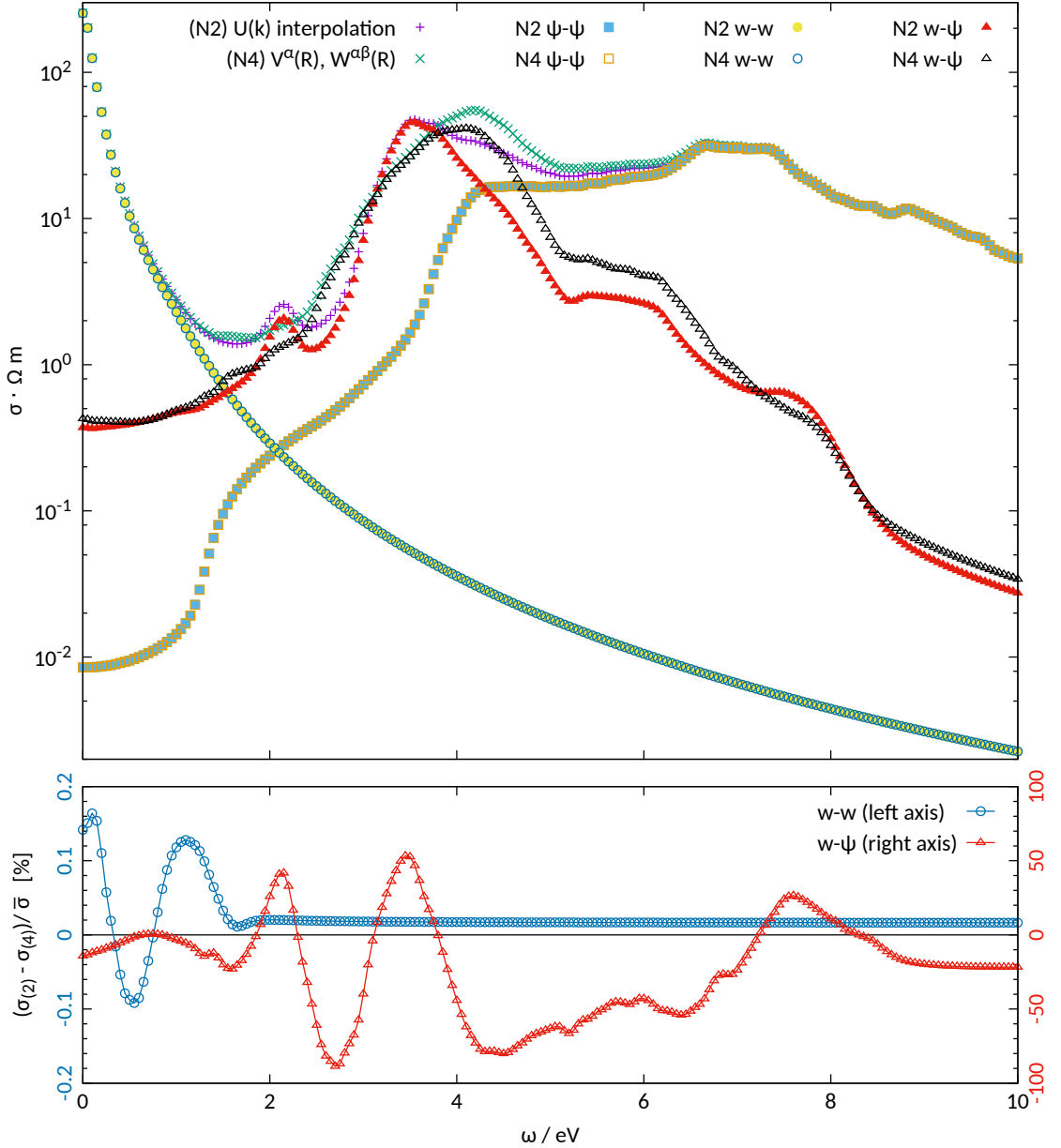


Figure 13: Contributions to the noninteracting optical conductivity on a uniform k -mesh, using momentum matrix elements from `optic` (with interpolated $\mathcal{U}(k)$; exact in this case), and from $V^\alpha(\mathbf{R}), W^{\alpha\beta}(\mathbf{R}, \omega)$. The lower panel shows the relative errors of the w-w and w- ψ contributions (note the different scales). The $\psi\psi$ contributions are identical by design.

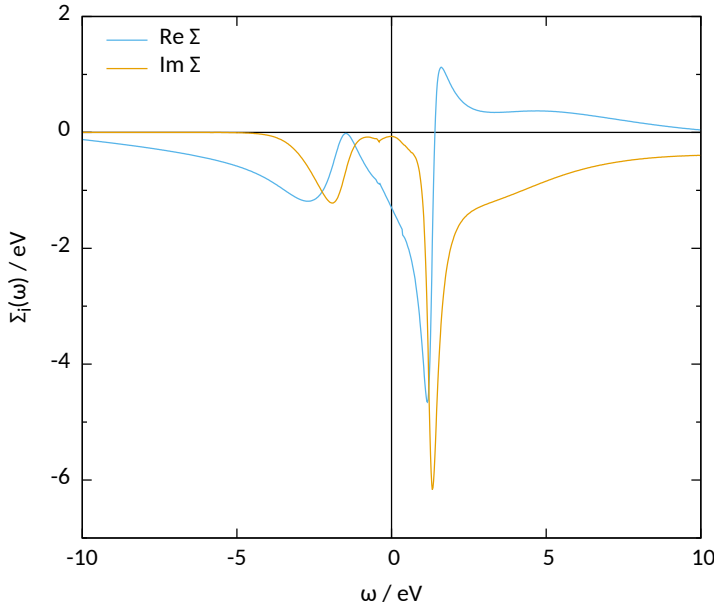


Figure 14: DMFT Self-energy of SrVO_3 , Wick-rotated to the real axis using maximum-entropy method (MAXENT) [Ass+15; Wis12]. The model is derived from a P-3 projection. Only the self-energy for one band is shown since the other two are identical within the uncertainties of the method.

- (i4) P-3 model with interpolated momentum matrix elements $V^\alpha, W^{\alpha\beta}$
- (i5) P-14 model with interpolated momentum matrix elements V^α
- (i6) P-14 with disentanglement and interpolated momentum matrix elements V^α

But note that (i2)/(i4) can no longer be expected to agree with (i3)/(i5), since the orbitals to which the self-energy is applied have different character.

Fig. 15 shows the optical conductivity of the P-3 model, the exact curve (i2) compared to (i4). Again, interpolation errors are clearly visible, albeit apparently smaller than in the noninteracting case. The individual contributions, shown in Fig. 16, reveal that this impression is somewhat misleading. In the region where the mixed transitions are important, the error is in fact similar, but it is masked by the w-w contribution, which is larger here than in the noninteracting case. On the other hand, the small peak at $\omega \approx 2 \text{ eV}$ in the w- ψ contribution is reproduced better in the interacting case.

Even with the ω -dependent self-energy included, the random-phase problem has so far been absent. This is because in this cubic material, the self-energy is orbital-independent (up to numerical accuracy from the quantum Monte Carlo (QMC) and analytic continuation), and therefore the argument from the diagonal

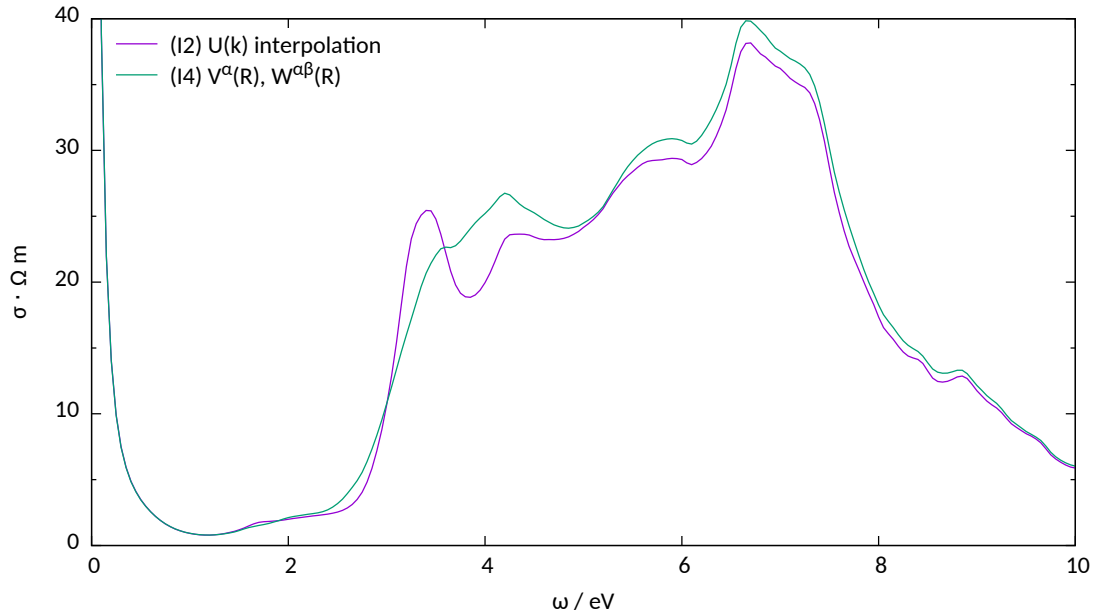


Figure 15: Optical conductivity for the interacting P-3 model computed on an adaptive k -grid using matrix elements from `optic` (with interpolated $\mathcal{U}(k)$; exact in this case), and interpolated matrix elements.

spectral function in the Bloch basis still holds. Therefore, we have been able to use the results with momentum matrix elements from `optic` as a reference against which the results from interpolated matrix elements could be compared.

Turning to P-14, this situation is reversed. Since we have satisfied ourselves that the Wannier interpolation for V^α is accurate, and since no mixed transitions are involved, we can rely on (15) as a reference, while (13) suffers from the random-phase problem. These results are shown in Fig. 17. In comparison with Fig. 15, the errors introduced by the random-phase problem and those introduced by the $W^{\alpha\beta}$ interpolation are similar in magnitude. The effect of disentanglement on (16) is quite similar to the noninteracting case (Fig. 12).

Using the original $\mathcal{U}(k)$

Up to now, the only results for the interacting P-14 model that can be considered reliable have come from matrix element interpolation (15). For independent confirmation, the original $\mathcal{U}(k)$ constructed by Wannier90 can be used together

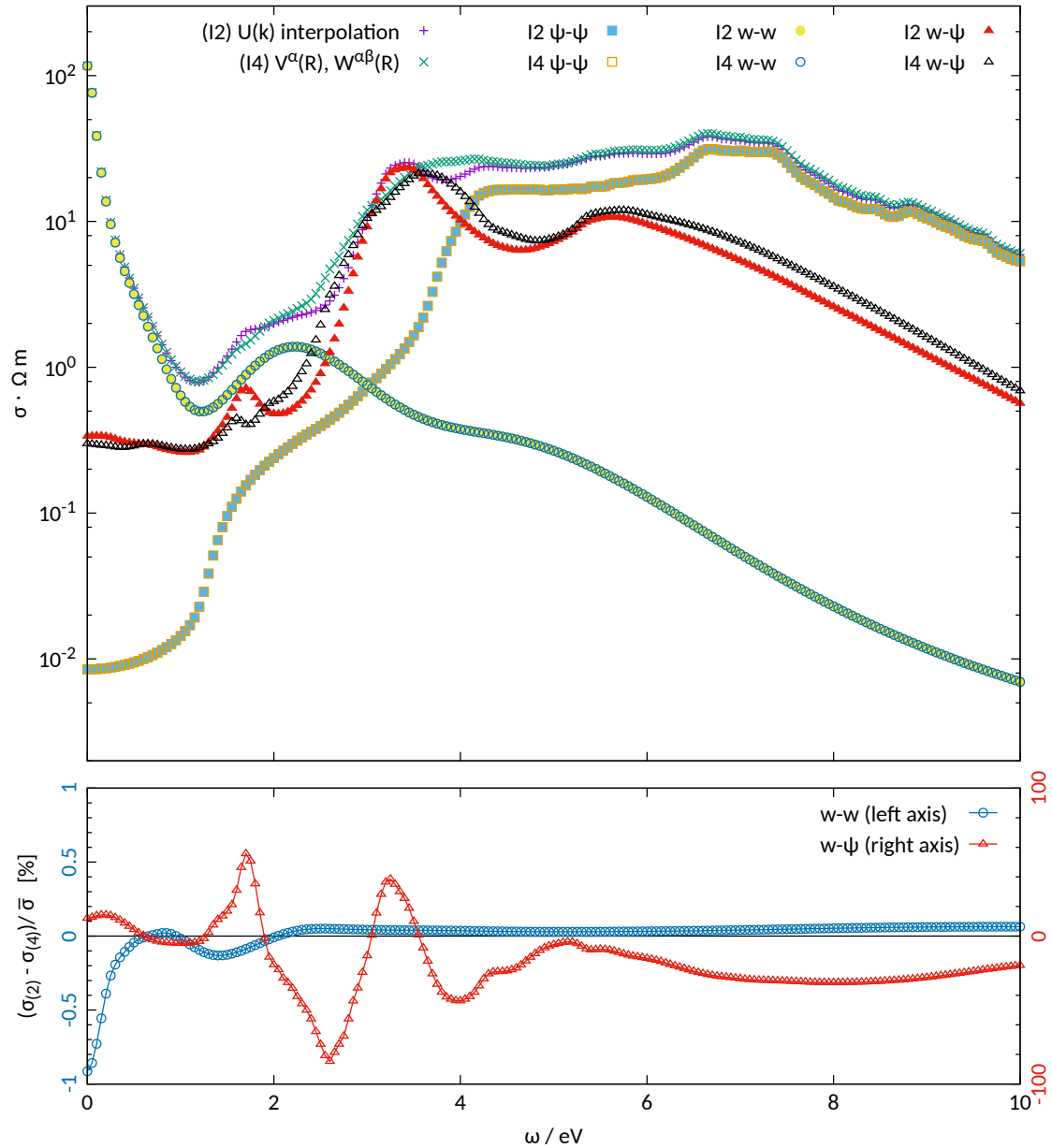


Figure 16: Like Fig. 13, but including a nontrivial self-energy.

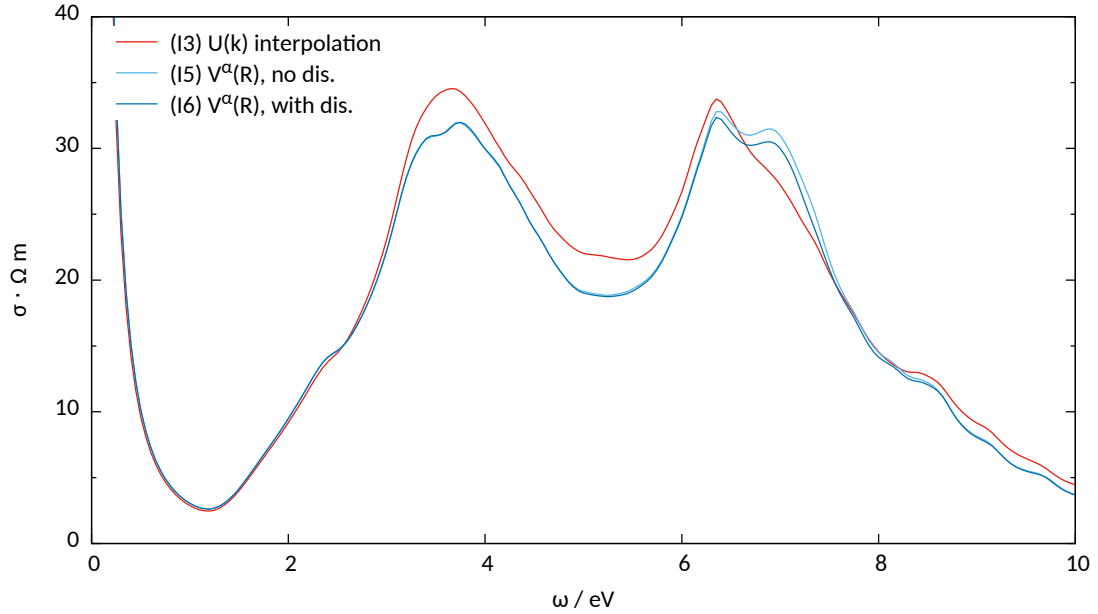


Figure 17: Optical conductivity for the interacting (unphysical) p-14 model computed using matrix elements from *optic* (with interpolated $\mathcal{U}(k)$), and interpolated matrix elements (exact in this case), with and without disentanglement.

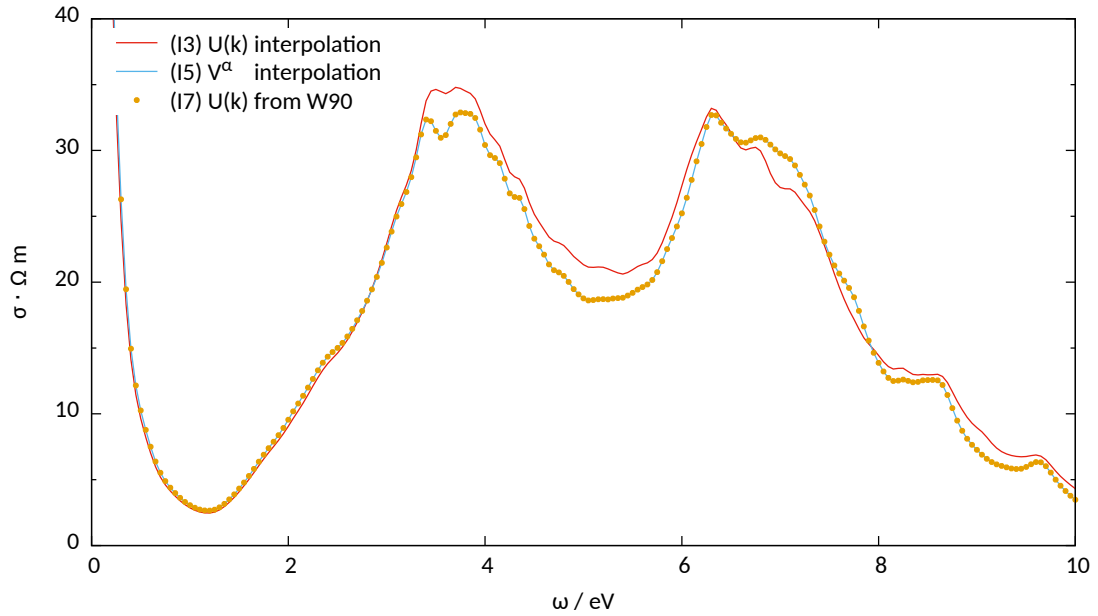


Figure 18: Optical conductivity for the interacting p-14 model computed with the original $\mathcal{U}(k)$ compared to the “standard” methods on the same k-grid. This calculation was done on a $16 \times 16 \times 16$ k-grid.

with the momentum matrix elements on the same k-mesh, thus ensuring that all the phases fit together. This approach is impractical for production usage because only the Wannier k-mesh can be used, which is a severe restriction for the optical conductivity; but as a test case, it will serve.

In Fig. 18, the curve

- (17) P-14 model with momentum matrix elements from `optic` and $\mathcal{U}(k)$ from Wannier90 — orange dots.

is indistinguishable from the result obtained with V^α interpolation (15). We may conclude that the differences between (13) and (15) are indeed due to the random-phase problem.

4 Discussion and outlook

WOPTIC is an algorithm and program package to calculate optical conductivities and related quantities from WIEN2k+DMFT calculations. With the relevant theory and the adaptive k-integration already in place [Ass+15; Wis12], the remaining obstacle was the random-phase problem that appeared because of the need to interpolate the WF to k-points not included in the original Wannier k-mesh.

Wannier interpolation of the momentum matrix elements V_{uv}^α proved a reliable and practical solution as far as transitions within the Wannier subspace are concerned. However, the generalization to Wannier-Bloch transitions is somewhat problematic. In the typical case where all bands that cross the Fermi level are described by the WF, this means that the problem affects only the optical conductivity, since for the static quantities (dc conductivity and thermopower), only Wannier-Wannier transitions are relevant.

The random-phase problem is absent when the self-energy is orbital independent, either by symmetry or because there is no DMFT self-energy (i.e., correlations are treated on the DFT level). When this restriction is relaxed, the numerical tests presented here indicate that errors from the phase problem and from Wannier interpolation of the mixed transitions are comparable. In either case, the important qualitative features of the optical conductivity are preserved. In practical LDA+DMFT calculations, the errors must be seen with respect to uncertainties stemming from the impurity solver and the analytic continuation of the self-energy, which can easily be dominant.

Finally, note that the random-phase problem is not caused by the adaptive integration as such. For practical purposes, the k-mesh on which the optical conductivity is integrated has to be finer than the Wannierization k-mesh, and the matrix elements on additional k-points are required, be it on a uniform or an adaptive grid. Also, the problem is not in principle limited to the optical conductivity. Any quantity that depends on the phases of the wf (through some matrix element $O_{uv}(k)$ which is not paired with $O_{vu}(k)$) would be similarly affected.

A complete solution to the random-phase problem would likely necessitate moving away from MLWF, e.g. to projector wf [Ani+05; Ku+02], which are fast to compute on arbitrary k-points (including disentanglement), or possibly the recently proposed *optimized projection function method* [Mus+15].

Apart from that, potentially fruitful directions for future work on WOPTIC include

- Incorporating disentanglement in the general case. Currently, cases with disentanglement are limited to Wannier-Wannier transitions as described in Sec. 2.3. However, given our observations in Sec. 2.3, it is unclear how this would be done.
- More straightforward is the generalization to a k-dependent self-energy $\Sigma(k, \omega)$ (e.g. from a GW calculation). This requires no change in the WOPTIC formalism, only an interpolation of the self-energy to the new k-points.
- In a more theoretical vein, it is unclear why the mixed momentum matrix elements $W^{\alpha\beta}$ are essentially real-valued and as localized as they are.

References

- [Ani+05] V. I. Anisimov, D. E. Kondakov, A. V. Kozhevnikov, I. A. Nekrasov, Z. V. Pchelkina, J. W. Allen, S.-K. Mo, H.-D. Kim, P. Metcalf, S. Suga, et al. "Full orbital calculation scheme for materials with strongly correlated electrons." *Phys. Rev. B* **71**, 125119 (2005). (Cit. on p. 29).
- [ASo06] C. Ambrosch-Draxl and J. O. Sofo. "Linear optical properties of solids within the full-potential linearized augmented planewave method." *Comput. Phys. Commun.* **175**, 1 (2006). (Cit. on p. 6).
- [Ass+15] E. Assmann, P. Wissgott, J. Kuneš, A. Toschi, P. Blaha, and K. Held. "woptic: optical conductivity with Wannier functions and adaptive k-mesh refinement." (2015). Submitted. (Cit. on pp. 1, 21, 22, 24, 28).
- [Ass15] E. Assmann. "Spectral properties of strongly correlated materials." PhD thesis. Vienna, Austria: Technische Universität Wien, 2015. (Cit. on p. i).
- [Har10] M. Hartl. *No, really, pi is wrong: The Tau Manifesto*. Tau Day. 2010. URL: <http://tauday.com/tau-manifesto> (visited on 08/20/2014). (Cit. on p. 5).
- [Ku+02] W. Ku, H. Rosner, W. E. Pickett, and R. T. Scalettar. "Insulating Ferromagnetism in $\text{La}_4\text{Ba}_2\text{Cu}_2\text{O}_{10}$: An Ab Initio Wannier Function Analysis." *Phys. Rev. Lett.* **89**, 167204 (2002). (Cit. on p. 29).
- [Kun+10] J. Kuneš, R. Arita, P. Wissgott, A. Toschi, H. Ikeda, and K. Held. "Wien2wannier: From linearized augmented plane waves to maximally localized Wannier functions." *Comput. Phys. Commun.* **181**, 1888 (2010). (Cit. on p. 2).
- [Lie03] A. Liebsch. "Surface versus Bulk Coulomb Correlations in Photoemission Spectra of SrVO_3 and CaVO_3 ." *Phys. Rev. Lett.* **90**, 096401 (2003). (Cit. on p. 2).
- [Mar+12] N. Marzari, A. A. Mostofi, J. R. Yates, I. Souza, and D. Vanderbilt. "Maximally localized Wannier functions: Theory and applications." *Rev. Mod. Phys.* **84**, 1419 (2012). (Cit. on pp. 7, 18).
- [Mos+08] A. A. Mostofi, J. R. Yates, Y.-S. Lee, I. Souza, D. Vanderbilt, and N. Marzari. "WANNIER90: A tool for obtaining maximally-localised Wannier functions." *Comput. Phys. Commun.* **178**, 685 (2008). (Cit. on p. 18).

References

- [Mus+15] J. I. Mustafa, S. Coh, M. L. Cohen, and S. G. Louie. “Automated construction of maximally localized Wannier functions: the optimized projection functions (OPF) method.” arXiv:1508.04148 [cond-mat] (2015). (Cit. on p. 29).
- [Nek+05] I. A. Nekrasov, G. Keller, D. E. Kondakov, A. V. Kozhevnikov, T. Pruschke, K. Held, D. Vollhardt, and V. I. Anisimov. “Comparative study of correlation effects in CaVO_3 and SrVO_3 .” Phys. Rev. B 72, 155106 (2005). (Cit. on p. 2).
- [Pal01] R. Palais. “ π is wrong!” Math. Intell. 23, 7 (2001). (Cit. on p. 5).
- [Pav+04] E. Pavarini, S. Biermann, A. Poteryaev, A. I. Lichtenstein, A. Georges, and O. K. Andersen. “Mott Transition and Suppression of Orbital Fluctuations in Orthorhombic $3d^1$ Perovskites.” Phys. Rev. Lett. 92, 176403 (2004). (Cit. on p. 2).
- [Pav+05] E. Pavarini, A. Yamasaki, J. Nuss, and O. K. Andersen. “How chemistry controls electron localization in $3d^1$ perovskites: a Wannier-function study.” New J. Phys. 7, 188 (2005). (Cit. on p. 2).
- [PBE96] J. P. Perdew, K. Burke, and M. Ernzerhof. “Generalized Gradient Approximation Made Simple.” Phys. Rev. Lett. 77, 3865 (1996). (Cit. on p. 2).
- [Rib+14] T. Ribic, E. Assmann, A. Tóth, and K. Held. “Cubic interaction parameters for t_{2g} Wannier orbitals.” Phys. Rev. B 90, 165105 (2014). (Cit. on pp. 2, 3).
- [Sca+14] A. Scaramucci, J. Ammann, N. A. Spaldin, and C. Ederer. “On the calculation of crystal field parameters using Wannier functions.” arXiv:1405.3804 [cond-mat] (2014). (Cit. on pp. 2, 3).
- [Sek+04] A. Sekiyama, H. Fujiwara, S. Imada, S. Suga, H. Eisaki, S. I. Uchida, K. Takegahara, H. Harima, Y. Saitoh, I. A. Nekrasov, et al. “Mutual Experimental and Theoretical Validation of Bulk Photoemission Spectra of $\text{Sr}_{1-x}\text{Ca}_x\text{O}_3$.” Phys. Rev. Lett. 93, 156402 (2004). (Cit. on p. 2).
- [Tar+13] C. Taranto, M. Kaltak, N. Parragh, G. Sangiovanni, G. Kresse, A. Toschi, and K. Held. “Comparing quasiparticle $GW+\text{DMFT}$ and $LDA+\text{DMFT}$ for the test bed material SrVO_3 .” Phys. Rev. B 88, 165119 (2013). (Cit. on p. 2).
- [Tom+12] J. M. Tomczak, M. Casula, T. Miyake, F. Aryasetiawan, and S. Biermann. “Combined GW and dynamical mean-field theory: Dynamical screening effects in transition metal oxides.” EPL 100, 67001 (2012). (Cit. on p. 2).
- [Wis+12] P. Wissgott, J. Kuneš, A. Toschi, and K. Held. “Dipole matrix element approach versus Peierls approximation for optical conductivity.” Phys. Rev. B 85, 205133 (2012). (Cit. on p. 1).

References

- [Wis12] P. Wissgott. “Transport Properties of Correlated Materials from First Principles.” PhD thesis. Vienna: Technische Universität Wien, 2012. (Cit. on pp. 1, 5, 7, 21, 22, 24, 28).
- [Yat+07] J. R. Yates, X. Wang, D. Vanderbilt, and I. Souza. “Spectral and Fermi surface properties from Wannier interpolation.” Phys. Rev. B 75, 195121 (2007). (Cit. on p. 7).